

EFFECTS OF A FOREST CLEARING: AN EXPERIMENTAL AND NUMERICAL ASSESSMENT

Tetsuya Nakamura, Koji Fukagata

Department of Mechanical Engineering, Keio University, Yokohama, Japan
tetsuya@kth.se

Antonio Segalini, P. Henrik Alfredsson

Linné Flow Centre, KTH Mechanics, Stockholm, Sweden

Numerical simulations are currently going on and therefore the numerical results will be shown and discussed in a revised version of the paper. We apologize for this inconvenient due to our mistake in the numerical simulations time planning.

ABSTRACT

The flow above a forest model with and without the presence of a clearing is investigated experimentally in a wind tunnel facility by means of Particle Image Velocimetry. The results have been analyzed in terms of basic velocity statistics and vertical integral length scale and a comparison of the two geometries is presented. In order to improve the current flow understanding and to complement the experimental results, Large Eddy Simulations of the same flows under similar operating conditions are planned. The experimental results indicate that the clearing is associated to a velocity defect in the mean velocity profile associated with a significant vertical momentum flux. The turbulence is redistributed amongst the various velocity components so that the streamwise velocity variance is reduced while the vertical velocity variance is enhanced. From the clearing windward edge the turbulence mixing contributes to the decrease of the vertical correlation length that increases again after the clearing trailing edge.

Introduction

There is a renewed interest in the wind estimate over forest areas due to the increasing demand of wind energy resources. Generally speaking, it is ideal to locate wind farms over off-shore or flat lands, where wind conditions are suitable for wind power production. However, the number of such suitable areas is limited, pushing the wind energy community to investigate complex terrains and, in particular, forested areas for which the available flow description is not as established as over smooth lands. While a description of the expected velocity profile as function of the various parameters, like roughness length or Obukhov length, has been investigated in the past (see for instance Harman & Finnigan, 2007), much less is known about the details of the turbulent field and how that is modified by the presence of the forest (Irvine *et al.*, 1997; Finnigan, 2000; Pietri *et al.*,

2009; Segalini *et al.*, 2013).

While the parameters affecting the homogeneous canopy flow are the geostrophic wind and the forest properties (forest height, permeability, leaf area density distribution, local drag coefficient, tree density), the presence of even a simple two-dimensional clearing introduces a number of additional parameters, like the clearing starting position and the clearing width, complicating the analysis further. Many investigations of forest clearings were performed experimentally (Bergen, 1975; Raupach *et al.*, 1987; Miller *et al.*, 1991; Nieveen *et al.*, 2001; Sanz Rodrigo *et al.*, 2007) and numerically (Dupont & Brunet, 2008), while at the moment the only analytical model developed to account for the effect of different forest endings is the one proposed by Belcher *et al.* (2003).

The main purpose of the present experimental and numerical effort is to characterize the flow over the ending position of the forest clearing, which is of particular interest due to the pressure strain imparted to the turbulent field. The experimental data obtained from a wind tunnel experiment will be compared with Large Eddy Simulations (LES) under similar forest conditions to complement the experimental results and to provide insight into the physical mechanisms of turbulence dynamics close to forest canopies. While the experimental data have been carefully scrutinized, the setup of the numerical simulations is ongoing and further results will be included in a revised version of the present manuscript.

Experimental setup

The experiments were performed in the Minimum Turbulence Level (MTL) wind tunnel at KTH in Stockholm. The MTL wind tunnel is a closed loop wind tunnel with a 7 m long test section, 0.8 m high and 1.2 m width. A schematic description of the experimental setup is shown in Figure (1) and more details have been reported by Segalini *et al.* (2013). In order to simulate the thick atmospheric boundary layer, four triangular spires were installed at the inlet of the test section, followed by a 3 m long aluminum mesh. The canopy model consists of four wooden flat plates. Each plate size is (width) \times (length) = 1.2 m \times 0.5 m, and it has 3500 holes in a staggered layout. Wooden cylindrical pins (diameter ϕ = 5 mm) were clamped in these

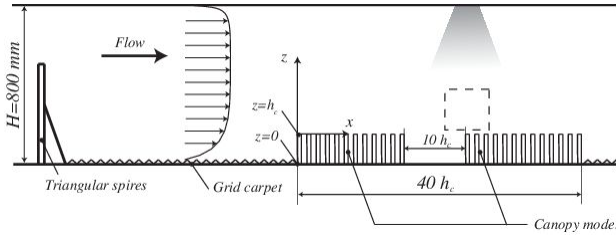


Figure 1. Schematic description of the experimental PIV setup.

holes to mimic a homogeneous high density forest (1700 pins/m²). The height of the canopy is $h_c = 50$ mm, and the total length of the forest model is $40h_c$.

Two cases were experimentally investigated, one with a full forest configuration and the other with the presence of a clearing that starts from $x/h_c = 20$ and ends at $x/h_c = 30$, where x is a streamwise coordinate that starts at the forest windward edge. The free-stream velocity was kept constant to about $U_\infty \approx 5$ m/s and in the following it will be used as the reference velocity scale, since the friction velocity (a more appropriate quantity in the roughness sublayer) cannot be easily measured in this non-equilibrium flow.

Particle Image Velocimetry (PIV) was performed with the commercial software *DaVis*. One high-speed C-MOS camera (Fastcam APX RS, 3000 fps at full resolution, 1024×1024 pixels, Photron) was positioned in backward-forward scattering mode at an angle of approximately 90° to the acquisition plane. Planar velocity snapshots were taken in the range with $29 \leq x/h_c \leq 32$ and $1.5 \leq z/h_c \leq 5.5$ with a sampling frequency of $f = 500$ Hz. The PIV data over the homogeneous forest case have been discussed by Segalini *et al.* (2012) where the measurements were compared with independent hot-wire anemometry data, demonstrating good agreement between the two measurement techniques and validating the present canopy model as representative of a real forest.

LES setup

Large Eddy Simulations (LES) are going to be performed soon to complement the experimental information. By applying a spatial filter on the nondimensional momentum equation, the filtered momentum equation can be written as

$$\frac{\partial \tilde{u}_i}{\partial t} + \tilde{u}_j \frac{\partial \tilde{u}_i}{\partial x_j} = -\frac{\partial \tilde{p}}{\partial x_i} + \frac{1}{Re} \frac{\partial^2 \tilde{u}_i}{\partial x_j \partial x_j} - \frac{\partial \tau_{ij}^{SGS}}{\partial x_j} - C_d A_f \sqrt{\tilde{u}_j \tilde{u}_j} \tilde{u}_i \quad (1)$$

where u_i is velocity, t is time, x_i ($x_1 = x$, $x_2 = y$, $x_3 = z$) are the streamwise, spanwise and vertical coordinates, and p is the air pressure. The buoyancy force and the Coriolis force are neglected, because our objective is to simulate the wind-tunnel experiment under a neutrally stratified condition. The Reynolds number is $Re = U_\infty \delta / \nu$, where U_∞ is the freestream velocity, δ is the 99% boundary layer thickness, and ν is the dynamic viscosity of the air. The Reynolds number is set to be $Re = 1.7 \times 10^5$ in this study.

The subgrid stress tensor τ_{ij}^{SGS} is modelled through an

SGS eddy viscosity model as

$$\tau_{ij}^{SGS} = u_i \tilde{u}_j - \tilde{u}_i \tilde{u}_j = -v_T^{SGS} \left(\frac{\partial \tilde{u}_i}{\partial x_j} + \frac{\partial \tilde{u}_j}{\partial x_i} \right) \quad (2)$$

Here v_T^{SGS} is the eddy viscosity, and it can be calculated similarly to Dupont & Brunet (2008), i.e. $v_T^{SGS} = 0.1 \sqrt{k} l$, where k is the SGS turbulent kinetic energy and l is a characteristic grid length scale. The length scale l is calculated as $l = (\Delta x \Delta y \Delta z)^{1/3}$.

The last term in right hand side of the Eq. (1) is the canopy drag term, where C_d and A_f represent the averaged canopy drag coefficient and the nondimensional leaf area per unit volume, with the usual notation. The typical value of the drag coefficient is $C_d = 0.2$, and that of the Leaf Area Index (LAI) is 5-9. In this study we use LAI = 6.

The SGS turbulent kinetic energy k is obtained by solving the transport equation

$$\frac{\partial k}{\partial t} + \tilde{u}_j \frac{\partial k}{\partial x_j} = -\tau_{ij}^{SGS} \frac{\partial \tilde{u}_i}{\partial x_j} + \frac{\partial}{\partial x_j} \left(2v_T^{SGS} \frac{\partial k}{\partial x_j} \right) - C_\epsilon \frac{k^{3/2}}{l} - 2C_d A_f \sqrt{\tilde{u}_j \tilde{u}_j} k \quad (3)$$

where $C_\epsilon = 0.93$ is the constant for the dissipation term.

The computational domain is composed of two parts: One is a driver part, where the inflow as a neutral boundary layer is generated, similarly to Lund *et al.* (1998), and the other is the main part, where the clearing effects on the canopy flow are going to be analyzed. The size of each domain ($L_x \times L_y \times L_z$) is ($20h_c \times 10h_c \times 20h_c$) and ($60h_c \times 10h_c \times 20h_c$) for the driver part and the main part, respectively, where L represents the length in each direction. The number of grids ($N_x \times N_y \times N_z$) is ($200 \times 100 \times 120$) for the driver part and ($600 \times 100 \times 120$) for the main part. The grid size ($\Delta x \times \Delta y \times \Delta z$) is ($0.1h_c \times 0.1h_c \times 0.1h_c$) below $z/h_c = 5$, while above this threshold the height of the grid is stretched with 2 percent stretching rate. In both the driver and the main domain, the upper boundary condition for the streamwise velocity u , the spanwise velocity v , and the vertical velocity w are imposed as $\partial u / \partial z = \partial v / \partial z = \partial w / \partial z = 0$, while no-slip condition is imposed at the ground surface boundary. Constant mass flux is applied at the inflow boundaries. The convective boundary condition is applied at the downstream end of each computational domain, and the periodic boundary conditions are imposed at the spanwise boundaries.

The Finite Difference Method (FDM) is used in the LES code. The staggered grid system, where the velocities are calculated at the cell surface while pressure and turbulent kinetic energy are located at the cell center, is used for the present code. The governing equations (Eqs. (1) and (3)) are temporally integrated using the low-storage Runge-Kutta scheme, while a divergence-free condition for the velocity is imposed by coupling pressure field with velocity. The coupling is done by solving the Poisson equation of the pressure. All derivative terms in the equations are discretized with second-order central finite difference scheme.

Two LES computations are planned to be done. One of them is full-forest configuration where the canopy drag is applied everywhere below $z/h_c = 1$ at $0 \leq x/h_c \leq 40$ in the main part, while the other has a clearing region at $20 \leq x/h_c \leq 30$ in order to have a similar configuration as the experimental setup.

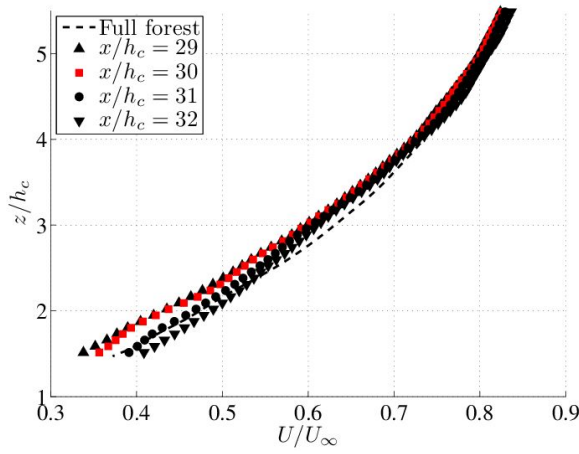


Figure 2. Mean streamwise velocity profiles at different axial stations over the clearing. The red symbols indicate the axial station of the clearing trailing edge. The dashed line indicates the homogeneous forest result.

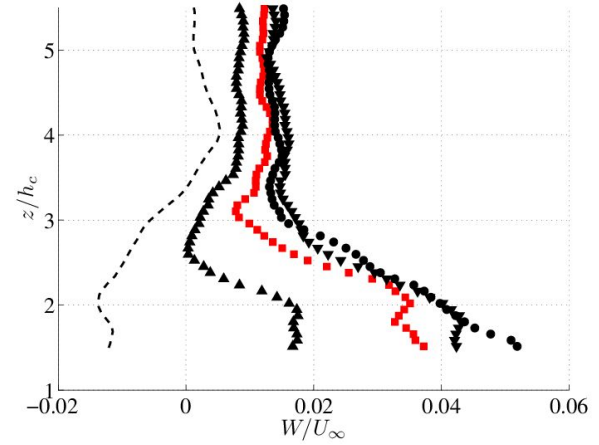


Figure 3. Mean vertical velocity profiles at different axial stations over the clearing. See the caption of Figure 2 for the nomenclature.

Experimental results

The mean streamwise and vertical velocity profiles at different axial positions along the clearing are shown in Figures (2) and (3), respectively. The first thing that can be noted is that the presence of the clearing is associated to a decrease in the streamwise velocity (compared to the homogeneous case). The velocity deficit decreases consistently when the flow is over the forest again and ejection of flow from the canopy top has place. This is further demonstrated by inspection of the vertical velocity profiles: While in the homogeneous forest case the vertical velocity is slightly negative due to the presence of the forest model trailing edge (located at $x/h_c = 40$), the presence of the clearing modifies this picture and the velocity becomes positive and keeps increasing even above the canopy, achieving a maximum approximately at $x/h_c \approx 31$. The picture that seems to emerge is that after the clearing windward edge, momentum is transferred downward, reducing the momentum available above the canopy. Vice versa, at the clearing trailing edge, the pressure strain due to the drag imparted by the canopy model, forces the flow to lift up: Some fluid parcels penetrate the canopy model but some are subsequently ejected in order to establish the balance between the flow shear and the canopy drag. This process is quite fast and reaches its maximum intensity about 1-2 h_c from the clearing trailing edge.

Figures (4) and (5) show the profiles of the streamwise and vertical velocity standard deviation, u'_{rms} and w'_{rms} respectively, demonstrating that the presence of the clearings provides a sink to the u'_{rms} , that appears significantly reduced compared to the full forest case up to about $z \approx 2 - 3h_c$, while the vertical standard deviation appears to be significantly enhanced. However, no clearing effect can be observed above $z/h_c = 3$ for neither mean velocity components nor the turbulence, thereby limiting the need of a model for the clearing effect only to the roughness sublayer.

Figures (6) and (7) show the streamwise velocity correlations at different height, and integral length scales at each x position, where the definition for each of them is written as

$$R_{uu} = \frac{\overline{u'(x,z)u'(x,z+\Delta z)}}{u'_{rms}(x,z)u'_{rms}(x,z+\Delta z)} \quad (4)$$

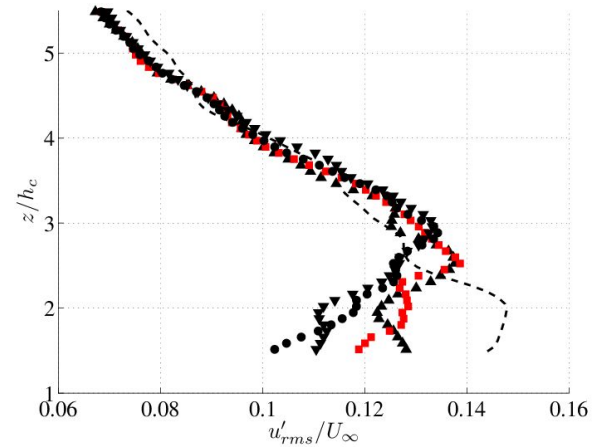


Figure 4. Streamwise velocity standard deviation profiles at different axial stations over the clearing. See the caption of Figure 2 for the nomenclature.

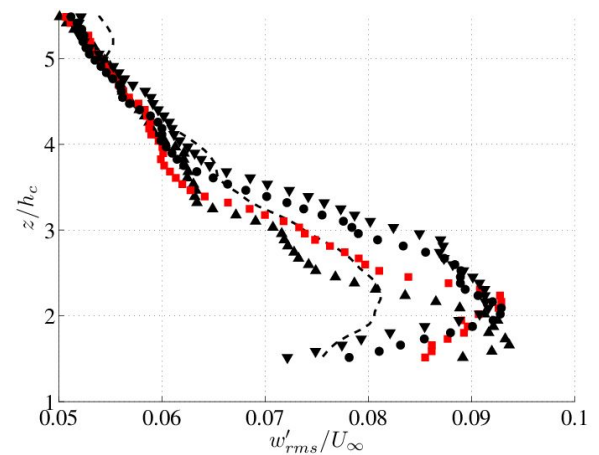


Figure 5. Vertical velocity standard deviation profiles at different axial stations over the clearing. See the caption of Figure 2 for the nomenclature.

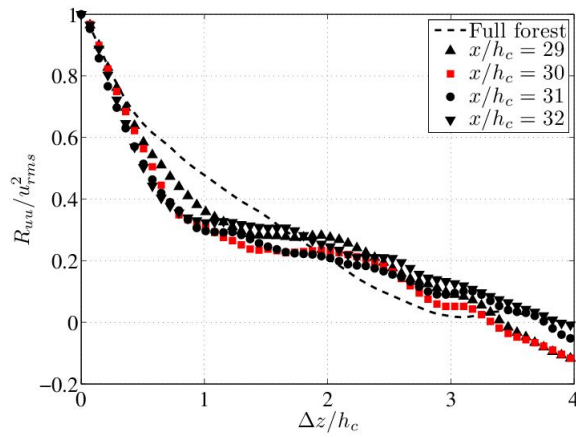


Figure 6. Two-point correlations profile in vertical (z) direction. See the caption of Figure 2 for the nomenclature.

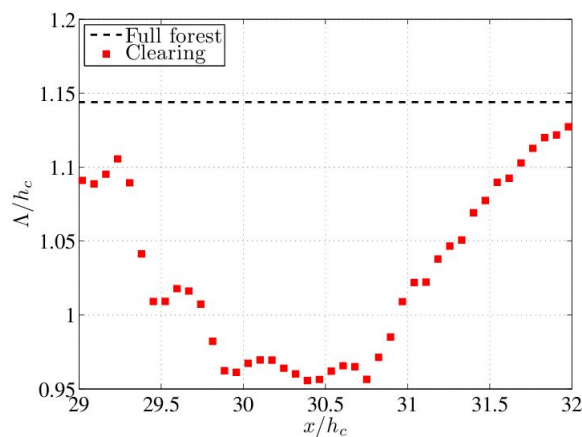


Figure 7. Integral length scale at each x position. The reference point is at the lowest position ($z_{ref}/h_c \approx 1.5$).

$$\Lambda = \int_0^{\max(\Delta z)} R_{uu} dz \quad (5)$$

It is possible to see that two-point correlations decay faster with the vertical separation distance when there is the clearing. Especially, one can see a slightly more rapid correlation decay from $\Delta z/h_c \approx 0.5$ to $\Delta z/h_c \approx 1$. This faster decay is associated to a reduced integral length scale shown in Figure (7): After the clearing windward edge, turbulence mixing is acting to facilitate the penetration of momentum downward and this phenomenon is associated to a reduction of the vertical correlation of the turbulent fluctuations. This process is interrupted close to the clearing trailing edge, where the pressure strain forces the flow to lift up gradually approaching the homogeneous forest state again.

Conclusions

The flow above a forest model with and without the presence of a clearing is investigated experimentally in a wind tunnel facility by means of Particle Image Velocimetry (PIV). In order to complement the experimental results, Large Eddy Simulations of the same flows under similar operating conditions are planned.

The experimental results indicate that the clearing is associated to a velocity defect in the mean velocity pro-

file associated with a significant vertical momentum flux. The turbulence is redistributed amongst the various velocity components so that the streamwise velocity variance is reduced while the vertical velocity variance is enhanced. The streamwise velocity variance is in fact damped due to the absence of the canopy drag from $x/h_c = 20$, while enhanced vertical velocity fluctuations can be observed at the end of the clearing. However the effects are limited below $z/h_c = 3$, which means the clearing effect is only dominant in the roughness sublayer at least for the neutral atmospheric conditions.

The clearing perturbation seems to be associated to turbulent mixing at its initial stage near $z \approx h_c$, followed by a rapid distortion near the clearing trailing edge. This phenomenon is highlighted by the low value of the vertical correlation length scale that, after the clearing trailing edge rises again towards to homogenous forest condition.

REFERENCES

- Belcher, S. E., Jerram, N. & Hunt, J. C. R. 2003 Adjustment of a turbulent boundary layer to a canopy of roughness elements. *J. Fluid Mech.* **488**, 369–398.
- Bergen, J. D. 1975 Air movement in a forest clearing as indicated by smoke drift. *Agricultural Meteorology* **15**, 165–179.
- Dupont, S. & Brunet, Y. 2008 Edge flow and canopy structure: a large-eddy simulation study. *Boundary-Layer Meteorol.* **126**, 51–71.
- Finnigan, J. J. 2000 Turbulence in plant canopies. *Annu. Rev. Fluid Mech.* **32**, 519–571.
- Harman, I. N. & Finnigan, J. J. 2007 A simple unified theory for flow in the canopy and roughness sublayer. *Boundary-Layer Meteorol.* **123**, 339–363.
- Irvine, M. R., Gardner, B. A. & Hill, M. K. 1997 The evolution of turbulence across a forest edge. *Boundary-Layer Meteorol.* **84**, 467–496.
- Lund, T. S., Wu, X. & Squires, K. D. 1998 Generation of turbulent inflow data for spatially-developing boundary layer simulations. *J. Comp. Phys.* **140**, 233–258.
- Miller, D. R., Lin, J. D. & Lu, Z. N. 1991 Some effects of surrounding forest canopy architecture on the wind field in small clearings. *Forest Ecol. Manag.* **45**, 79–91.
- Nieveen, J. P., El-Kilani, R. M. M. & Jacobs, A. F. G. 2001 Behaviour of the static pressure around a tussock grassland-forest interface. *Agr. Forest Meteorol.* **106**, 253–259.
- Pietri, L., Petroff, A., Amielh, M. & Anselmetti, F. 2009 Turbulence characteristics within sparse and dense canopies. *Environ. Fluid Mech.* **9**, 297–320.
- Raupach, M. R., Bradley, E. F. & Ghadiri, H. 1987 Wind tunnel investigation into the aerodynamic effect of forest clearing of the nesting of abbotts booby on christmas island. *Progress Report, CSIRO Division of Environmental Mechanics, Canberra, Australia*.
- Sanz Rodrigo, J., van Beeck, J. & Dezsö-Weidinger, G. 2007 Wind tunnel simulation of the wind conditions inside bidimensional forest clear-cuts. application to wind turbine siting. *J. Wind Eng. Ind. Aerod.* **95**, 609–634.
- Segalini, A., Fransson, J. H. M. & Alfredsson, P. H. 2012 Turbulent structures in canopy flows. In *Proceedings of the Euromech colloquium “Wind Energy and the impact of turbulence on the conversion process”, 22-24 February 2012, Oldenburg, Germany*.
- Segalini, A., Fransson, J. H. M. & Alfredsson, P. H. 2013



August 28 - 30, 2013 Poitiers, France

Scaling laws in canopy flows: A wind-tunnel analysis.
Boundary-Layer Meteorol. pp. DOI 10.1007/s10546-

013-9813-2.